arXiv:physics/0502002v1 [physics.comp-ph] 1 Feb 2005

Density-functional studies of tungsten trioxide, tungsten bronzes, and related systems

B. Ingham[1], S.C. Hendy[1,2], S.V. Chong[2] and J.L. Tallon[1,2]
[1] *Victoria University of Wellington, P.O. Box 600, Wellington, New Zealand and*
[2] *Industrial Research Ltd., P.O. Box 31310, Lower Hutt, New Zealand*
(Dated: February 2, 2008)

Tungsten trioxide adopts a variety of structures which can be intercalated with charged species to alter the electronic properties, thus forming 'tungsten bronzes'. Similar optical effects are observed upon removing oxygen from WO_3, although the electronic properties are slightly different. Here we present a computational study of cubic and hexagonal alkali bronzes and examine the effects on cell size and band structure as the size of the intercalated ion is increased. With the exception of hydrogen (which is predicted to be unstable as an intercalate), the behaviour of the bronzes are relatively consistent. $NaWO_3$ is the most stable of the cubic systems, although in the hexagonal system the larger ions are more stable. The band structures are identical, with the intercalated atom donating its single electron to the tungsten *5d* valence band. Next, this was extended to a study of fractional doping in the Na_xWO_3 system ($0 \leq x \leq 1$). A linear variation in cell parameter, and a systematic change in the position of the Fermi level up into the valence band was observed with increasing x. In the underdoped WO_{3-x} system however, the Fermi level undergoes a sudden jump into the conduction band at around $x = 0.2$. Lastly, three compounds of a layered $WO_4 \cdot \alpha,\omega$-diaminoalkane hybrid series were studied and found to be insulating, with features in the band structure similar to those of the parent WO_3 compound which relate well to experimental UV-visible spectroscopy results.

INTRODUCTION

Tungsten trioxide has long been studied for its interesting structural, electronic, and electrochromic properties. Tungsten trioxide is most stable in a pseudo-cubic, distorted ReO_3 structure [1] but can also form metastable hexagonal [2], tetragonal [3] and pyrochlore [4, 5] structures. For all of these structures it is possible to intercalate mono- or di-valent cations in the vacancies or channels within the structures to form the so-called 'tungsten bronzes' [3, 6, 7, 8]. The resulting materials exhibit a continuous colour change [9] and often a large increase in the electrical conductivity, which becomes metallic in nature [10]. The most-studied system is that of the cubic alkali bronzes (M_xWO_3, M = Group I alkali ion, $0 \leq x \leq 1$). Of these, the sodium bronze is the only compound that has been reported with $x = 1$ [9], however in the hexagonal system, all alkali ions (Li - Cs) have been intercalated to varying degrees [1]. In the cubic system, even low levels of doping ($x < 0.2$) cause a dramatic colour change, which has led to tungsten trioxide being used as a material in electrochromic windows [11, 12, 13]. Bulk superconductivity has been observed at 2-3 K in $Na_{0.2}WO_3$ [14]. In addition to electronic doping, tungsten trioxide can also exhibit electron-doping via the removal of oxygen, with similar colouration effects [15]. However colouration and conduction are not strictly related, as the conductivity in a thin film of oxygen-deficient WO_{3-x} is much lower than in a thin film of M_xWO_3 of the same colour [16]. This indicates that the mechanism for mobility is not simply due to delocalised electrons or holes, but rather changes in the band structure near the Fermi level, which are different for the two types of material [16, 17]. Recent work by our group has concentrated on developing organic-inorganic hybrid materials based on two-dimensional tungsten oxide sheets (formed by corner-shared WO_6 octahedra) linked with organic diamine molecules [18, 19]. The electronic structure of these materials will determine how they may be used in various electronic applications. This work presents *ab initio* computations on a variety of tungsten oxide derivatives, including a series of cubic and hexagonal alkali tungsten bronzes, variable doping Na_xWO_3 ($0 \leq x \leq 1$), oxygen-deficient WO_{3-x}, and some simple layered organic-inorganic tungsten oxide hybrid structures to aid in understanding the optical and electronic properties of the latter. During the course of completing this work another paper has recently appeared which treats some of the earlier materials [20].

COMPUTATIONAL DETAILS

We have applied density functional theory (DFT) within the generalized gradient approximation (GGA) [21] using the VASP package [22, 23, 24, 25] which solves the DFT-GGA Kohn-Sham equations within the pseudopotential approximation. Here the valence electrons have been expanded in a plane wave basis set and the effect of the core on the valence electrons has been modelled with ultrasoft pseudopotentials. We used ultrasoft Vanderbilt type pseudopotentials [26] as supplied by G. Kresse and J. Hafner [27]. The pseudopotential valence states and cut-off energies for all elements used are given in Table I.

To study the effect of fractional doping in the Na_xWO_3 system, we used a supercell method consisting of up to eight primitive WO_3 cells, with between 1-7 of these cells

TABLE I: Pseudopotential parameters used for all calculations.

Atom	Valence Electrons	Cut-off energy (eV)
W	$6s^1 5d^5$	188.192
O	$2s^2 2p^4$	395.994
H	$1s^1$	200.000
Li	$2s^1$	76.254
Na	$3s^1$	48.686
K	$4s^1$	70.923
Rb	$5s^1$	63.093
Cs	$6s^1$	47.697
C	$2s^2 2p^2$	286.744
N	$2s^2 2p^3$	348.097

occupied by sodium ions in a pseudo-random fashion. Similarly for the oxygen-deficient WO_{3-x} system, 3-6 cells were used with one oxygen vacancy in each case. In all cases the basis vectors of the cell were chosen to avoid the creation of lines or planes of dopants.

k-point meshes between 4×4×4 and 15×15×15 were used to relax the various systems, corresponding respectively to 24-36 and 120-455 k-points in the irreducible Brillouin zone. As a general rule, the simplest bronze structures with few (1-4) formula units per cell used finer k-point meshes (more k-points) than the larger non-metallic WO_{3-x} and hybrid structures. In all cases the k-point mesh was varied at the end of the relaxation and the energy was found to converge to better than 10 meV in all cases. The cell parameters and atomic positions were allowed to relax in alternate cycles. The atomic positions were considered relaxed when the total energy had converged to within 10 meV between ionic steps. In the calculations of the hybrid structures the relative positions of the in-plane tungsten and oxygen atoms were fixed at the origin and half-way along each planar axis, respectively.

CUBIC AND HEXAGONAL ALKALI BRONZES

Structure

The alkali elements (H, Li, Na, K, Rb and Cs) were each used as the intercalated species in cubic MWO_3 ($x = 1$ bronzes) and hexagonal $M_{0.33}WO_3$ (full intercalation of the hexagonal tunnels). In each case the intercalated metal atom was placed in the plane of the apical oxygen atoms, in the centre of the cavity (Figure 1). WO_3 does not form a perfectly cubic cell at room temperature, as the WO_6 octahedra are slightly distorted in terms of W−O bond lengths and W−O−W bond angles, due to antiferroelectric displacement of the tungsten atoms and subsequent rotation of the WO_6 octahedra [1, 28]. However this is not taken into account in the calculated system; the cell always relaxes to a cubic structure. In calculations involving supercells of tungsten trioxide the distortions are seen [20]. Tungsten bronzes on the other hand do form the simple cubic structure at high intercalation levels [29]. The hexagonal structure, which was also studied for comparison, is the same for both the oxide and bronzes. (The term 'cubic' is used connotatively throughout this article of those systems that are cubic or close to it; as opposed to the hexagonal systems also studied.)

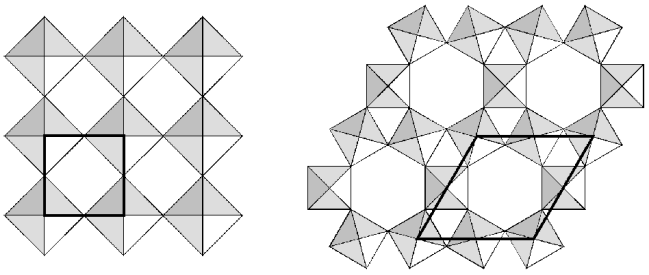

FIG. 1: The structure of cubic (left) and hexagonal (right) tungsten oxide and bronzes. The unit cell is indicated in each case.

Figure 2 shows some experimental results for the cubic bronze system (obtained from [29, 30, 31, 32]. In the case of non-cubic WO_3 a cubic cell was calculated from the volume average of the given parameters.) Of all the intercalated alkali elements which have been attempted experimentally, only sodium is able to form a stable structure with $x = 1$ at normal temperatures and pressures. In general the calculated cell parameters for the cubic system are larger than the experimental. It is also noticeable that as the size of the intercalated ion increases, the cell size increases super-linearly. The Goldschmidt tolerance factor for cubic perovskites can be calculated from the formula $t = \frac{r_M + r_O}{\sqrt{2}(r_W + R_O)}$ [33], where r_j are the ionic radii. For a perovskite structure to be stable, t must be less than unity. The tolerance factors for $NaWO_3$ and KWO_3 are 0.909 and 1.056 respectively, indicating that

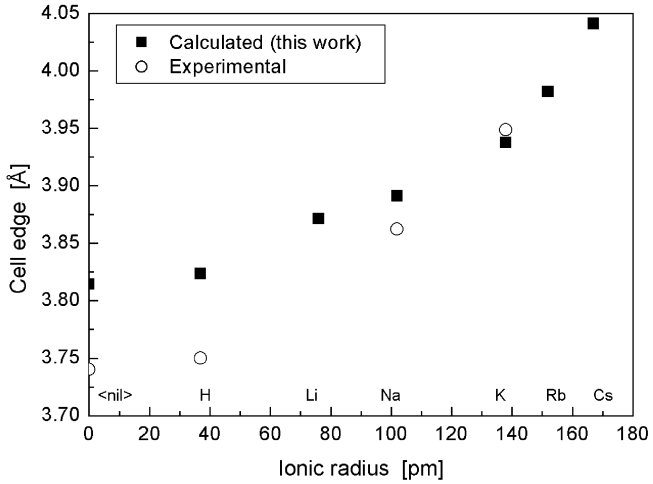

FIG. 2: Calculated and experimental values of the cell parameter for fully intercalated cubic tungsten bronzes.

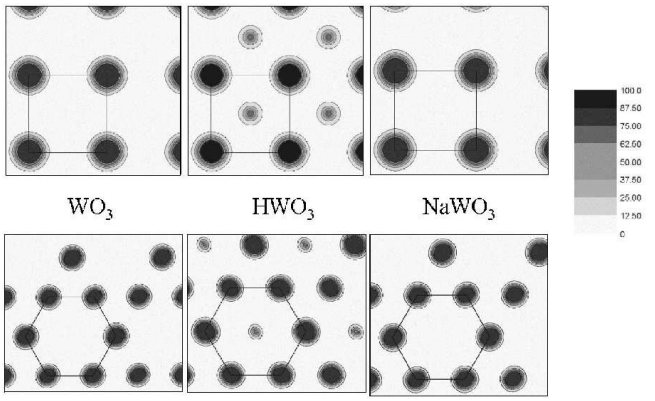

FIG. 3: Charge density maps of cubic (top) and hexagonal (bottom) tungsten oxide and bronzes. The largest tunnels are indicated, which are completely filled in each case. The oxygen atoms in-plane with the intercalated atom can be clearly seen, and only in the case of hydrogen is the charge still associated with the intercalated atom.

the potassium atom is slightly too large to form a stable structure. Potassium bronzes have been formed with high x contents, but only under high-pressure synthesis conditions [32]. Rubidium and caesium cubic bronzes with high x content cannot be formed. The hexagonal structure, having larger tunnels, is able to accommodate larger ions than observed in the cubic system. In the experimental system the stability of hydrogen is notoriously difficult to maintain, as it is quite mobile due to its small size. Both hydrogen and lithium are small enough ions to be able to occupy the small triangular sites between the hexagonal tunnels [1]. Thus reported experimental results for H^+- and Li^+-hexagonal bronzes may show differing behaviour from larger atoms because the occupied sites may be different in each case. In the experimental hexagonal system, the a parameter is observed to increase as ions are intercalated while the c parameter decreases. The final values are relatively consistent across the series, as given in Table II. These are generally lower than the calculated values we have obtained, although most discrepancies are less than 0.5%.

For the hexagonal system, the changes in the lattice parameters are much less pronounced than in the cubic system, as shown in Table III. This is due to the hexagonal tunnel spaces being much larger than the cavities in the cubic system and so the interactions between the inserted ion and the WO_3 lattice are smaller.

Charge density

Charge density plots of the cubic system taken in a plane through the centre of the cell where the intercalated atom sits, reveal that hydrogen behaves differently from the other intercalates. This is shown in Figure 3. Bearing in mind that the charge density plots consider only the valence electrons, the fact that we observe some charge on the hydrogen atom but not on any of the others indicates that hydrogen is not ionised. That larger atoms are completely ionised is consistent with other reported experimental results [28]. It is interesting that the same phenomenon occurs in both the cubic and hexagonal cases. The first ionisation energy of the intercalates are as follows: hydrogen 1.318 eV, lithium 0.526 eV, sodium 0.502 eV, potassium 0.425 eV, rubidium 0.409 eV, caesium 0.382 eV [34]. The high ionisation energy of hydrogen with respect to the other intercalates may be responsible for the differing behaviour.

Energies of formation

The energies of formation of the cubic and hexagonal tungsten bronzes are shown in Table IV and Figure 4. These are calculated by subtracting the ground state energies of the components (WO_3 plus the metal cation) from the ground state energy of the final product (tungsten bronze). A negative energy of formation therefore indicates that the compound formed is stable.

Firstly, a comparison of cubic and hexagonal WO_3 shows that the hexagonal phase has a very similar energy to the cubic phase. Literature results indicate that the cubic phase is preferred, although the hexagonal phase is stable up to temperatures of 400-500^{o}C, indicating that the phase transition has a high activation energy [1, 2]. In both the cubic and hexagonal systems, the hydrogen-intercalated bronze energy is positive and large, indicating that the hydrogen bronzes are not stable. In the experimental system the hydrogen bronzes are easily oxidised as the protons are highly mobile [31, 35]. This result also relates to hydrogen being the only intercalate

TABLE II: Experimental cell parameters for hexagonal tungsten oxide and bronzes (from [1, 3]), compared with our calculated results for hexagonal tungsten bronzes with hexagonal sites completely occupied.

Compound	Experimental a (Å)	Calculated a (Å)	Experimental c (Å)	Calculated c (Å)
WO_3	7.298	7.4103	3.899	3.8144
$H_{0.33}WO_3$	7.38	7.4173	3.78	3.8111
$Li_{0.33}WO_3$	7.405	7.4007	3.777	3.8219
$Na_{0.33}WO_3$	7.38	7.4034	3.775	3.8248
$K_{0.33}WO_3$	7.37	7.4010	3.77	3.8282
$Rb_{0.33}WO_3$	7.38	7.4163	3.78	3.8289
$Cs_{0.33}WO_3$	7.38	7.4507	3.785	3.8342

TABLE III: Calculated cell volume per WO_3 unit for cubic and hexagonal tungsten oxide and bronzes.

Compound	Cubic (Å^3)	Hexagonal (Å^3)
WO_3	55.4977	60.4648
H_xWO_3 [a]	55.8946	60.5278
Li_xWO_3	58.0127	60.4270
Na_xWO_3	58.9116	60.5158
K_xWO_3	61.0457	60.6785
Rb_xWO_3	63.1294	60.7928
Cs_xWO_3	65.9809	61.4445

[a] $x = 1$ for cubic, $x = 0.33$ for hexagonal.

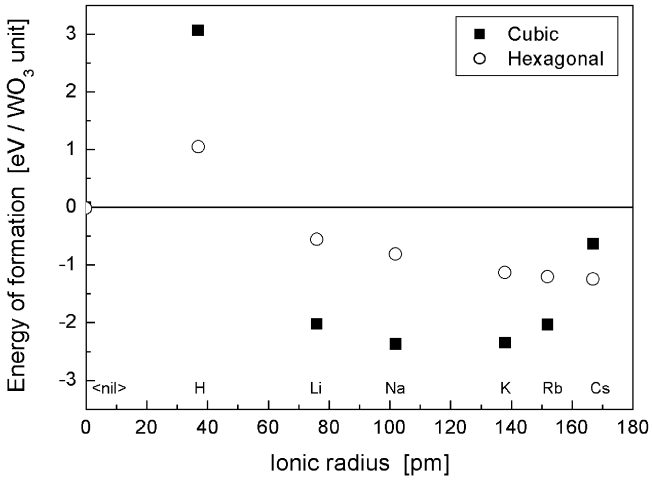

FIG. 4: Calculated energies of formation per WO_3 unit for cubic and hexagonal tungsten bronzes, relative to cubic WO_3.

that does not ionise in the bronze structures, as evidenced by the charge density plots earlier. For the hexagonal bronzes (apart from hydrogen) there is a steady downward trend in the energy of formation as the size of the intercalated alkali metal ion increases. Therefore the larger ions form more stable bronzes than the smaller ones, which is also indicated in the literature [3]. In the cubic system however, the energy drops to a point and then, beyond Na, increases in the case of the larger intercalates. This point coincides with the stability predicted by the Goldschmidt perovskite tolerance factor. For the stable compounds (WO_3, $LiWO_3$, and $NaWO_3$) there is a progressive decrease in the energy of formation. This supports experimental evidence that sodium may well be the most stable of the cubic bronzes, as it is the only one for which a fully intercalated compound has been reported [35].

Density of states

For both the cubic and hexagonal systems other than hydrogen, the basic band structures of the bronzes are essentially identical to the parent oxide of the same phase. The only difference amongst them is the position of the Fermi level relative to the valence and conduction bands, which will be discussed later. Hence comparing the band structure of hexagonal and cubic WO_3 will aid a great deal in describing the bronze systems. A comparison of the density of states for cubic and hexagonal WO_3 is shown in Figures 5 and 6. The lowest band, situated at -18 to -16 eV, corresponds to the oxygen 2*s* orbitals. This band is present in all of the tungsten-oxide-based systems studied to date and always occurs at the same energy regardless of the structure or the presence of intercalated atoms or molecules.

The broad valence band, from -7 to 0 eV, is comprised mainly of oxygen *2p* orbitals. There is a small tungsten

TABLE IV: Calculated energies of formation per WO_3 unit for cubic and hexagonal tungsten oxide and bronzes, relative to cubic WO_3.

Compound	Cubic(eV)	Hexagonal(eV)
WO_3	0	-0.016
H_xWO_3 [a]	3.059	1.047
Li_xWO_3	-2.023	-0.560
Na_xWO_3	-2.373	-0.813
K_xWO_3	-2.354	-1.132
Rb_xWO_3	-2.039	-1.203
Cs_xWO_3	-0.637	-1.245

[a] $x = 1$ for cubic, $x = 0.33$ for hexagonal.

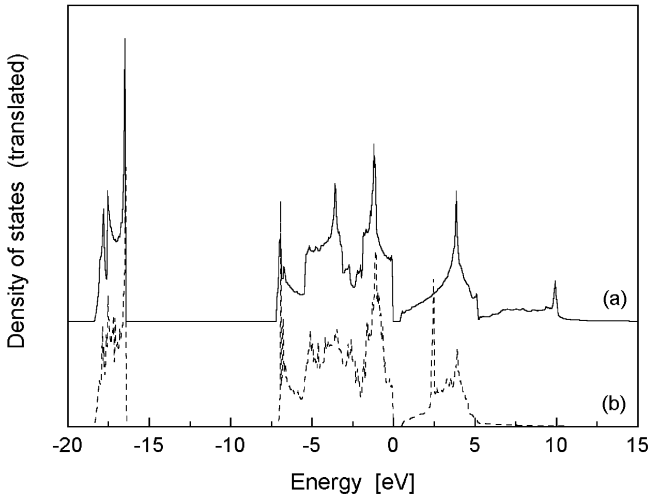

FIG. 5: The density of states as calculated for cubic (a) and hexagonal (b) WO_3.

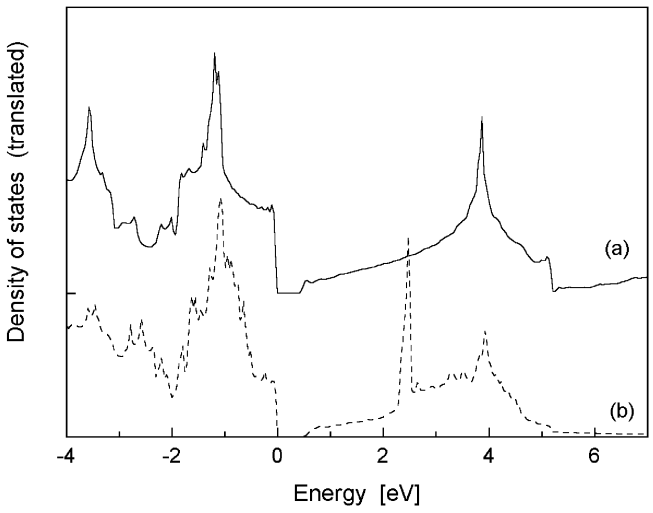

FIG. 6: A detailed view of the conduction band of cubic (a) and hexagonal (b) WO_3, from figure 5.

5d component but this is negligible above -2 eV. The valence band cut-off is sharp at 0 eV and coincides in both the cubic and hexagonal case with the Fermi level, rendering the oxide materials semiconducting. The conduction band, detailed in Figure 8, lies from 0.5 to 5 eV in both the cubic and hexagonal cases. In the cubic case it is solely comprised of tungsten *5d* orbitals; however in the hexagonal case there is also some additional oxygen *2p* contribution - particularly to the strong peak feature observed at 2.5 eV. The band gap (defined as the difference in energy between the top of the valence band and the bottom of the conduction band) is 0.4 eV in the cubic system and 0.5 eV in the hexagonal. This is much less than the observed band gap, which is typically reported in the range of 2.5 - 3 eV, and as being indirect [12, 36, 37]. However this is not too surprising as DFT generally underestimates band gaps. The presence of peak features in the density of states can also lead to the phenomenon where even though the conduction band is being filled, there is a sudden increase in the population of the conduction band at these peaks and a sharp transition in the optical spectrum is observed.

It is worth taking pause here to point out the similarities between this work and that of experimental results and other calculations reported on the same structures. X-ray photoelectron spectroscopy (XPS) reveals that the valence band is comprised of oxygen *2p* states only, and the conduction band of tungsten *5d* states [12, 38]. The oxygen *2s* state at $\sim$ -20 eV has also been observed by XPS [39] although, given the precision of the measurement, this band is broadened out and appears to extend into the oxygen *2p* valence band, the distinction of which is not made by the authors. Calculations using the local-density approximation and full-potential linear muffin-tin orbitals (where all electrons are considered, not just the valence electrons as in the case of the VASP program) result in density of states spectra which are virtually identical to those we have obtained [40, 41]. This is the case in both the cubic and hexagonal systems. An older paper by D.W. Bullet [28], utilising a non-relativistic atomic orbital-based method shows a very similar band structure

(oxygen *2p* as valence band and tungsten *5d* as conduction band).

Figure 7 shows a comparison of the density of states of the cubic bronzes with the parent oxide. The hydrogen bronze system shows a large peak feature at the bottom of the conduction band, which is attributed to the non-ionised hydrogen *1s* orbital. Because only one electron is contributed from the hydrogen, the Fermi level lies about in the middle of this sub-band. For the other bronze systems, analysis of the density of states contribution from each atom reveals that the intercalated atom contributes very little if at all to the overall density of states. This is expected due to its complete ionisation, as the single valence electron of the intercalated atom is contributed to the W−O framework [28]. All compounds have the Fermi level located well into the conduction band, rendering them metallic. The shape of the band structure does not change as atoms are intercalated. This is also noted in other literature [40, 41]. Also, the magnitude of the band gap and the position of the Fermi level is relatively constant - even for those compounds which are known to be unstable (cubic potassium, rubidium and caesium bronzes).

We have also derived the band structure curves along lines of symmetry in cubic WO_3 and cubic $NaWO_3$. These are given in Figure 8. These results agree extremely well with the calculated band structures of both Bullett [28] and Cora et. al. [41], considering that different methods were used for each calculation. We again notice the high degree of similarity between the parent oxide and the sodium bronze, with the only major difference being the position of the Fermi level.

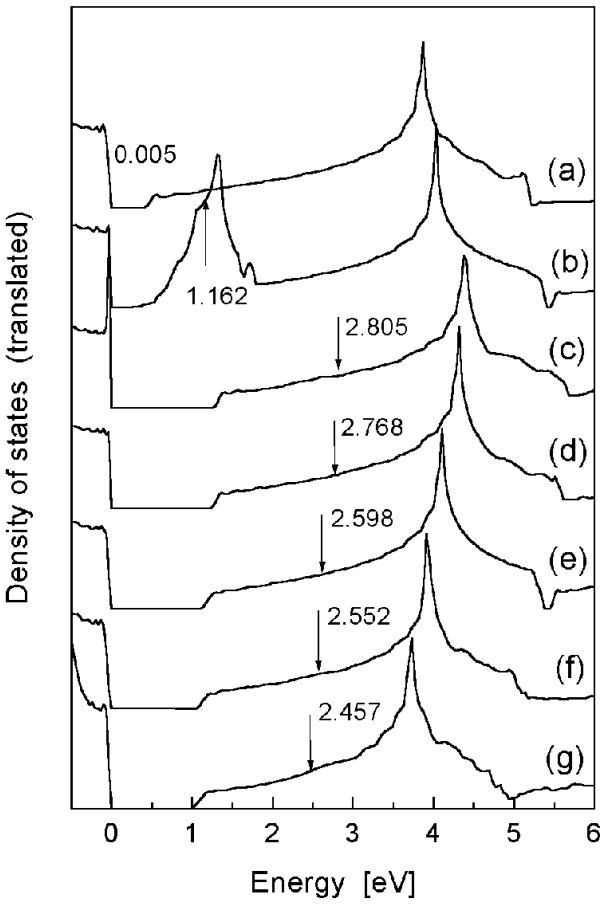

FIG. 7: Calculated density of states for cubic tungsten bronzes, MWO_3, near the Fermi level: (a) WO_3, (b) HWO_3, (c) $LiWO_3$, (d) $NaWO_3$, (e) KWO_3, (f) $RbWO_3$, (g) $CsWO_3$. The Fermi level is indicated in each case.

CUBIC SODIUM TUNGSTEN BRONZE SERIES

Following the work comparing cubic and hexagonal tungsten bronzes, we set out to explore the sodium bronze system more thoroughly. Experimentally it is quite difficult to obtain a completely saturated sodium tungsten bronze (i.e. $x = 1$), and even when an excess of sodium tungstate is used in the reaction $3x{\cdot}Na_2WO_4 + (6-4x)WO_3 + x{\cdot}W \rightarrow 6Na_xWO_3$, it is not a given that the resulting bronze will have $x = 1$ [29]. There is a raft of experimental results, however, on sodium bronzes with $x < 1$ (refs. [3, 9, 10, 29, 42], to name but a few), all illustrating that x is a continuous quantity and not confined to any series of exactly stoichiometric compounds. In addition to $x = 0$ and 1, which were performed as part of the cubic tungsten oxide and alkali bronze series, we have calculated the structure and density of states for $x = \frac{n}{8}; n = 1-8$. The average cubic cell parameter was found to increase linearly with x as shown in figure 9. Also shown in this figure is a series of reported experimental results. For higher x contents the two data sets are very close, with the calculated parameters being about 0.8% larger than the experimental; again, a good result given the approximations made using this method. However below $x = 0.3$, the experimental results differ markedly from the calculated values, due to a phase change to a tetragonal form at low x values in the experimental system [43]. The structure of the tetragonal phase is not related to the cubic phase [3]. It contains seven WO_3 units per cell (28 atoms), and when one takes the fractional doping into account, the resulting system quickly becomes much too large to attempt a calculation with the computational resources available to us. In the work of Walkingshaw et. al. [20] the volume versus x deviates from this linear behaviour for x as large as 0.5.

There are no obvious changes in the appearance of the density of states as x increases from zero to one. The nature of the band structure near the Fermi level is shown in figure 10. The band gap increases linearly with x, while the Fermi level quickly moves into the conduction band. According to this plot we would expect to see a semiconductor-metal transition at about $x = 0.06$, where the Fermi level moves into the conduction band. How-

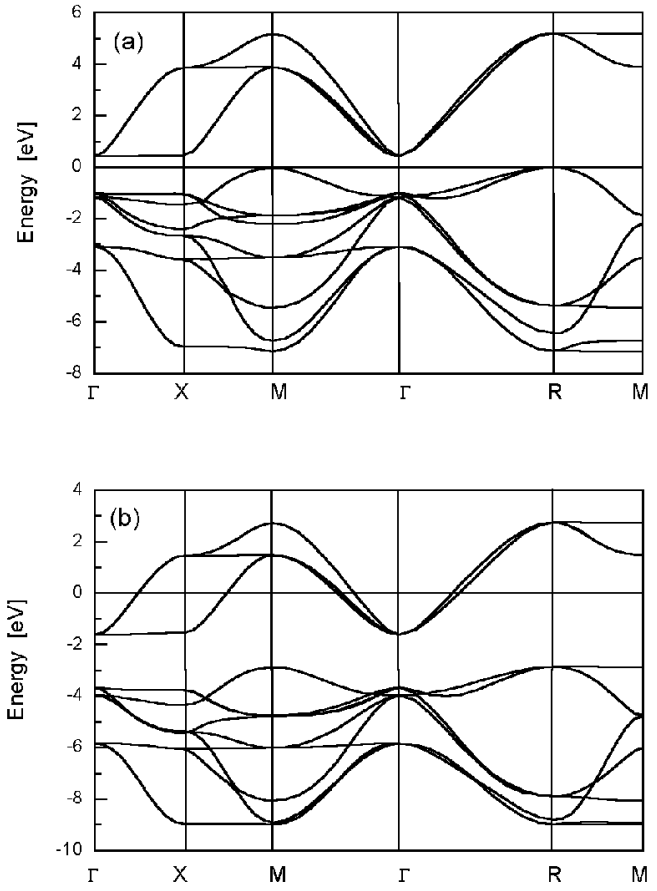

FIG. 8: Band structure diagrams of cubic WO_3 (a) and $NaWO_3$ (b).

ever, in the experimental system this transition is observed at $x = 0.3$, corresponding to (and perhaps influenced by) the structural transition ([3], and references therein).

Once again, analysis of the individual atomic contributions to the density of states indicates that each sodium atom is fully ionised, and the electron donated to the tungsten *5d* conduction band [28].

SUB-STOICHIOMETRIC WO_{3-x} SERIES

As a complement to the sodium bronze series, sub-stoichiometric WO_{3-x} was examined for compounds with x ranging from zero to 0.33. In the experimental system, the maximum oxygen loss that can be achieved without a drastic phase change is ~ 0.35 ([44], and references therein). There are a number of different stoichiometric formulae for compounds in the range $WO_{2.65}$ - WO_3, and for some of these the crystal structure has been solved. They are given the names α-, β- and γ-phase, as shown in Table V with their respective formulae. The crystal structures of the β- and γ-phases were solved by Magneli [45, 46]. Booth et al. generalise the β-phase even further by describing the existence of crystallographic shear planes [47]. This can account for the broad range of compositional formulae. While we are unable to calculate the properties of these phases as described in literature due to the restriction on the number of atoms in the system, we are able to observe the effect that removal of oxygen has on the simple cubic WO_3 phase.

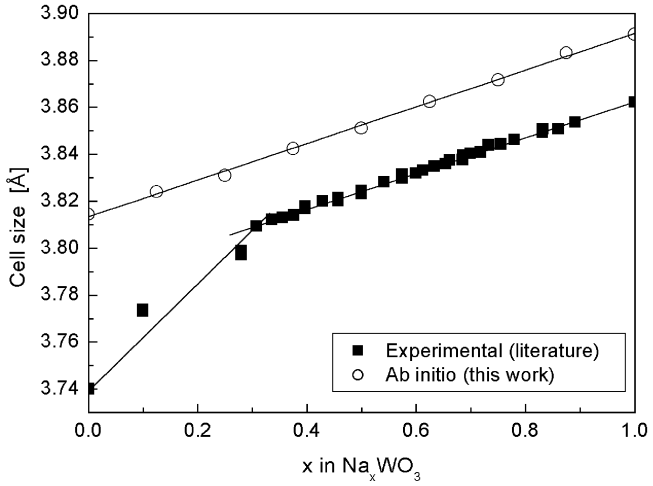

FIG. 9: Calculated and experimental values of cell parameter for cubic Na_xWO_3 with variable x.

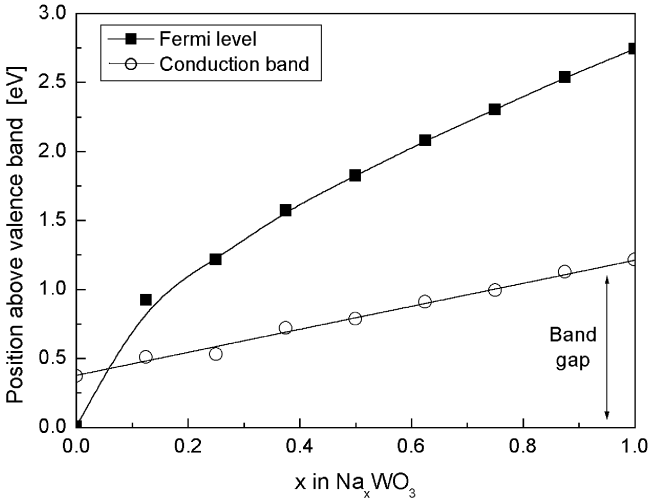

FIG. 10: Band structure of Na_xWO_3 near the Fermi level showing the movement of the Fermi level into the conduction band at low x values. The lines are given as a guide.

As one might expect, removing oxygen from a site causes a local distortion of atoms around the vacancy, and the cell ceases to be simple orthorhombic. The cell volume changes; initially there is a slight increase at low deficiencies, followed by a decrease. These results are shown in Figure 11 and are in good agreement with experimental values, despite the absence of the phase change in the calculated system.

The energies of formation for the different species stud-

TABLE V: Compositional ranges for sub-stoichiometric tungsten oxide species. From [44].

Phase	Formula	Range	Average
α	WO_3	$WO_{2.95}$ – WO_3	WO_3
β	$W_{20}O_{58}$	$WO_{2.88}$ – $WO_{2.94}$	$WO_{2.90}$
γ	$W_{18}O_{49}$	$WO_{2.65}$ – $WO_{2.76}$	$WO_{2.72}$
δ	WO_2	$WO_{1.99}$ – $WO_{2.02}$	WO_2

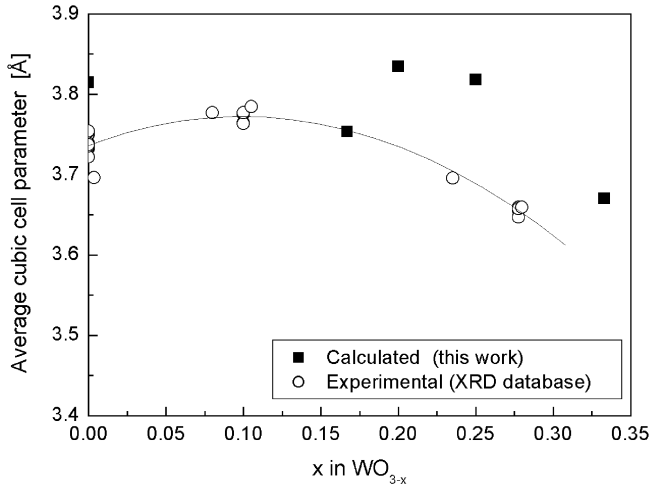

FIG. 11: The volume-averaged cubic cell parameter for calculated and experimental sub-stoichiometric 'cubic' WO_{3-x} systems. The curve is given as a guide.

ied are given in Table VI. We note that a slight deficit of oxygen ($x = \frac{1}{6}$) is more favourable energetically than stoichiometric WO_3. This is observed experimentally, as commercial WO_3 powder exhibits a loss of oxygen over 1-2 days in atmospheric conditions. Further loss of oxygen renders WO_{3-x} less energetically favourable than its parent oxide, and once again, as was the case with sodium tungsten bronzes, the presence of a phase change in the experimental system may explain any discrepancies seen.

It is also of interest to look at the changes in the density of states as oxygen is removed from WO_3. As mentioned in the introduction, oxygen-deficient WO_3 exhibits an increased conductivity, but not as great as that due solely to the presence of doped electrons. Figure 12 shows the density of states for the WO_{3-x} system in the region near the Fermi level. The overall spectra share the same features previously detailed for WO_3: the oxygen *2s* band near -18 eV; the broad valence band, comprised mainly of oxygen *2p* orbitals, from -7 to 0 eV; and the conduction band, consisting solely of tungsten *5d* orbitals, lying from roughly 0.5 to 5 eV. Naturally the sub-stoichiometric systems appear more 'jagged' than the parent WO_3 compound, due in part to the breaking of symmetry, rendering each atom non-equivalent to others within the cell, and causing its contribution to be slightly different.

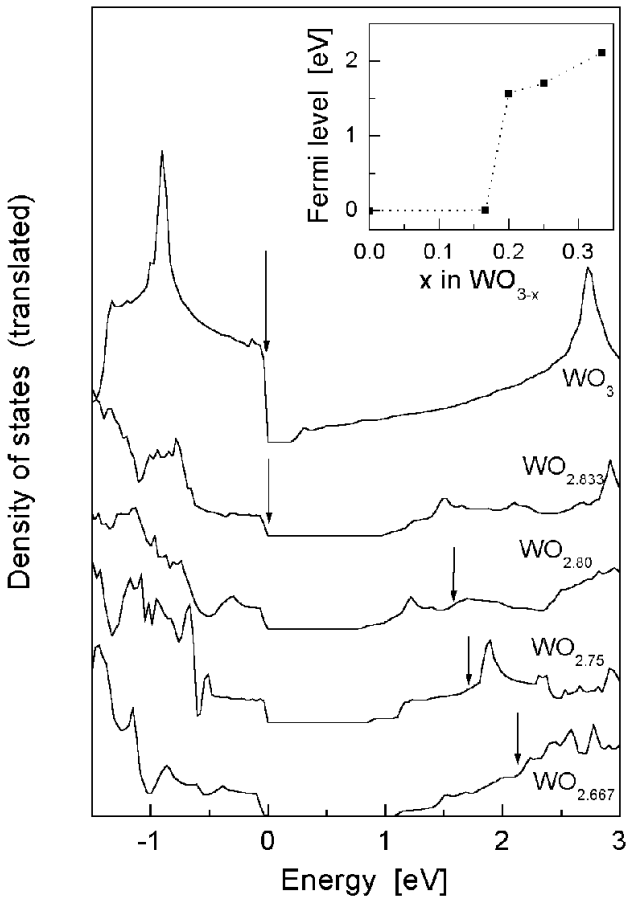

FIG. 12: Density of states for the WO_{3-x} system, all with the valence band set at zero. Arrows show the position of the Fermi level. Inset: Position of the Fermi level relative to the top of the valence band.

The inset of Figure 12 shows the progression of the Fermi level into the conduction band. There is a sharp jump between $x = 0.167$ and 0.2 as the Fermi level moves up into the conduction band - not a gradual transition as in the case of the sodium bronzes Na_xWO_3. While the $x = 0.167$ compound has the Fermi level at zero (and therefore, still non-conducting), the band structure of the valence band is similar to that of the conducting species. It appears that there is a decrease in the density of states in the valence band, followed by the Fermi level being pushed up into the conduction band. The stoichiometry

TABLE VI: Energies of formation of the calculated WO_{3-x} species calculated by the formula $E_F = E_{TOTAL} - \sum E_{PARTS} = E(WO_{3-x}) - (E(WO_3) - \frac{x}{2}E(O_2))$.

Formula	Energy of formation (eV/unit formula)
WO_3 $(x = 0)$	0
$WO_{2.833}$ $(x = \frac{1}{6})$	-0.103
$WO_{2.8}$ $(x = \frac{1}{5})$	0.447
$WO_{2.75}$ $(x = \frac{1}{4})$	1.007
$WO_{2.667}$ $(x = \frac{1}{3})$	1.661

at which this insulating-conducting transition occurs is in good agreement with the literature value of $WO_{2.76}$, which coincides with the β-γ structural phase transition [17].

ORGANIC-INORGANIC LAYERED HYBRIDS

Following on from the background studies of tungsten bronzes and the oxygen-deficient tungsten oxides, layered organic-inorganic hybrid compounds were studied. These structures consist of WO_4 layers (as in H_2WO_4 [48]), connected via aliphatic (linear) alkyl diamines. These have been investigated experimentally by us elsewhere [18]. Three different length alkyl amines were used in the calculations, with two, four and six carbons. The input structure of the hybrid systems is the most conceptually simple: a single unit formula, $WO_4{\cdot}H_3N(CH_2)_nNH_3$ ($n = 2, 4, 6$ - hereby abbreviated to W-DAn). It is highly conceivable that the calculated structure of the hybrid compounds is in a slightly higher energy state than that of the actual structure, which may be a supercell of the simple input case, with possible tilts and rotations of the octahedra and organic molecules. As mentioned, WO_3 does not form a simple cubic structure, but exhibits small distortions of bond lengths and angles which render it very slightly off-cubic, with eight formula units per cell. In extending the computations to the organic-inorganic systems then, several constraints were necessary. Firstly only one cell was used, which may affect the outcome not only due to the removal of distortion in the inorganic layer (which apparently lowers the energy in the oxide and hydrate compounds) but also because this does not allow for the differing orientation of the organic molecules in neighbouring cells. Secondly, constraints were placed on the inorganic atoms in order to maintain the position of the layer. This entailed fixing the position of the tungsten and planar oxygen atoms at the corner and edges of the cell respectively. This was sufficient to relax the atoms to a sensible structure.

These compounds are isomorphic with diaminoalkane metal halides which have been investigated by Mitzi [49]. There, two schemes were identified for the bonding of the organic ammonium group to the inorganic layer, designated 'bridging' and 'terminal' (which we shall call 'apical'). In the 'bridging' case the organic ammonium forms hydrogen bonds to two bridging and one apical atom (in the work of Mitzi, this is a halogen atom; in our work, oxygen) while in the 'apical' case hydrogen bonds are formed to two apical and one bridging atom (Figure 13). This causes the alkyl chain to lie diagonally within the cell when the ammonium group is in a bridging configuration, but parallel for the apical. When the alkyl chain is longer than one carbon (methylamine), the second carbon in the chain would be too close to the opposing apical (oxygen) atom if a bridging conformation were adopted. Thus in general, apical bonding is observed for organic-inorganic systems with organic chain lengths of two or more carbon atoms.

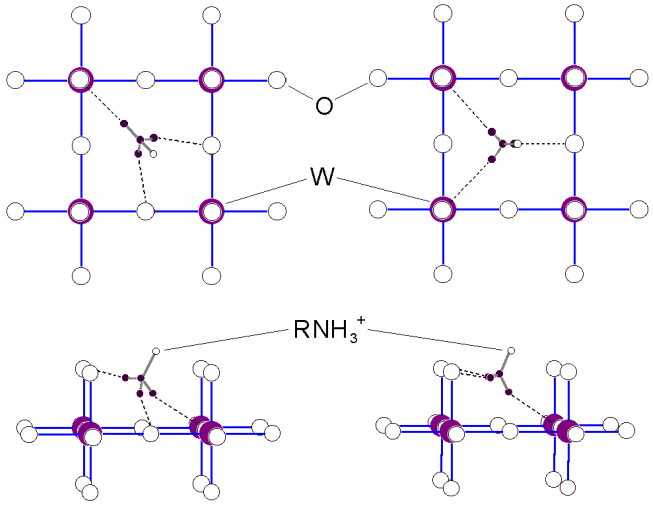

FIG. 13: Schematic diagrams illustrating the two bonding configurations, 'bridging' (left) and 'apical' (right), in organic-inorganic hybrid materials. Only the first carbon atom of the organic molecule is shown for simplicity.

Given this, calculations were initially performed on the methylamine system in both the bridging and apical configurations, to compare the energies of each and as a starting point to construct the initial cells for the computations of the longer chain diamine hybrids. Figure 14 shows the calculated relaxed structures of one methylammonium ion with respect to the tungsten oxide layer. In

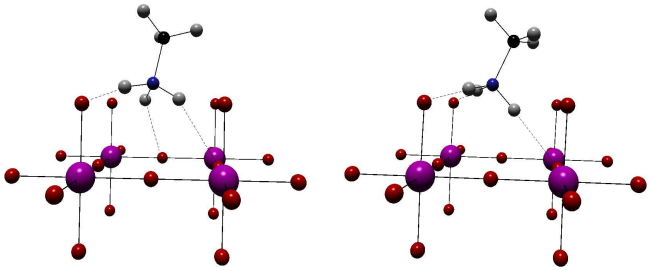

FIG. 14: Calculated structure of methylamine in bridging (left) and apical (right) configurations.

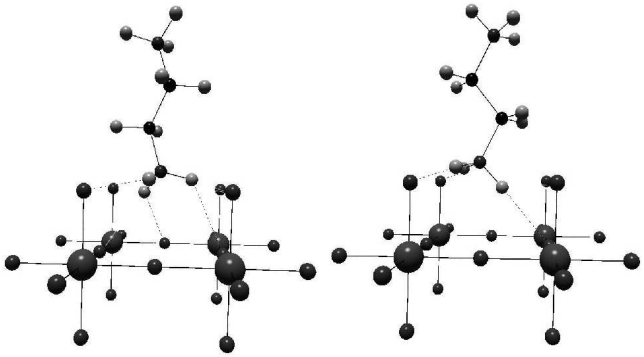

FIG. 15: Calculated structures of diaminoethane (DA2) in bridging (left) and apical (right) configurations.

both cases the calculated structure closely resembles that expected from the diagram in Figure 13. In the apical case the shortest hydrogen bonds between the ammonium hydrogen atoms and the oxygen atoms of the inorganic layer are as expected: two short hydrogen bonds to two apical oxygens and one to the opposing bridging oxygen. However, for the bridging case the two hydrogens that were expected to interact with adjacent bridging oxygens are actually closer to apical oxygens. In this latter case the tilting of the organic molecule is much less than for the apical case, and overall it appears that there is a more delocalised attraction between the hydrogen and oxygen atoms.

The energies of the two systems were calculated to be -123.31 eV for the apical case and -123.08 eV for the bridging. Thus the apical configuration appears to be more stable, both from its lower energy and examination of the structure with more localised forces. Each of the two methylamine structures were used as a basis for the initial positions of the diaminoethane (DA2) compound. The relaxed cell parameters are given in Table VII. In the apical case the cell volume is slightly less than in the bridging case. Despite the greater tilting expected for the terminal structure, the planar axes (a and c) are shorter and the interlayer spacing b is longer than for the bridging. The two structures are shown in Figure 15. As for the methylammonium structures, in the bridging conformation there are several longer bond distances from each hydrogen to the oxygen atoms, whereas in the apical conformation for each hydrogen there is a single bond that is distinctly shorter to one oxygen than the others.

The energies of these two structures are calculated to be -114.709 eV for the bridging conformation and -115.750 eV for the apical. The apical conformation is therefore more stable, and the difference between the two is greater than for the methylammonium case. Two other systems were extended from the apical W-DA2: W-DA4 (4-carbon chain) and W-DA6 (6-carbon chain). Again the planar tungsten and oxygen atom positions were fixed. The energies of formation are given in Table VIII. As can be seen from the negative values, all three compounds are stable, with W-DA4 being the least stable of the three. This seems to be confirmed experimentally as W-DA4 is harder to form than both W-DA2 and W-DA6.

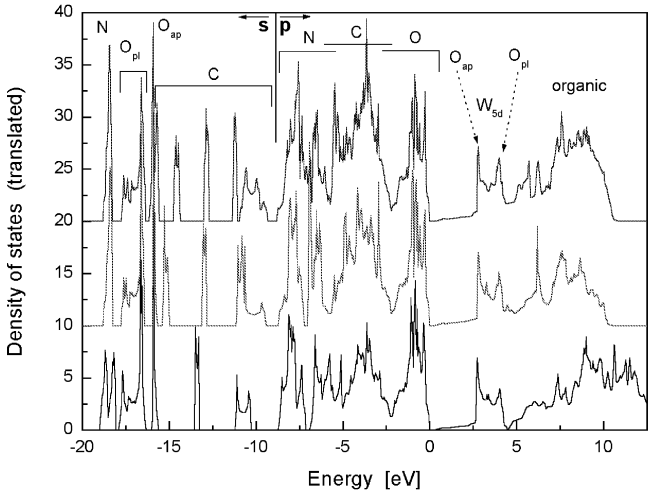

FIG. 16: Calculated density of states for W-DA2 (bottom), W-DA4 (middle) and W-DA6 (top). The Fermi level is located at E=0.

The density of states of the three compounds are all very similar. The results are shown in Figure 16. The main features are as follows: As in the tungsten oxide and tungsten bronze systems, the oxygen *2s* band is located between -18 and -16 eV. There is a splitting between the planar and apical oxygen contributions, with the planar oxygen bands being broader and lying at slightly lower energies. The nitrogen *2s* bands lie at about -18.5 eV and the carbon *2s* bands lie between -16 and -9 eV. The appearance of multiple carbon s bands in the longer chain systems is due to the different environments in which the carbon atoms are located along the length of the chain. Between -9 and 0 eV lie the *2p* bands of N (lowest), C (middle) and O (highest). The hydrogen atoms associated with the carbon and nitrogen atoms contribute their single *1s* electrons to the bands of their respective atoms.

The oxygen band, from -2 to 0 eV, closely resembles that of the tungsten oxides and bronzes. There is rela-

TABLE VII: Calculated cell parameters of W-DA2 with the organic molecule in the bridging and apical conformations.

	W-DA2 bridging	W-DA2 apical
a (Å)	3.9443	3.9108
b (Å)	8.7345	8.7992
c (Å)	3.9443	3.9245
α	89.98	89.99
β	90.02	90.01
γ	90.02	90.01
Volume (Å^3)	135.8266	135.0498

TABLE VIII: Energies of formation of the calculated W-DAn compounds, calculated by the formula $E_F = E_{TOTAL} - \sum E_{PARTS} = E(WO_4 \cdot H_3N(CH_2)_nNH_3) - (E(H_2WO_4) + E(H_2N(CH_2)_nNH_2))$.

Compound	Ground state energy (eV)	Ground state energy of organic molecule	Energy of formation
W-DA2	-115.750	-64.172	-0.939
W-DA4	-148.189	-97.506	-0.044
W-DA6	-181.887	-130.714	-0.534

tively little organic or tungsten component to this band, so once again the valence band is comprised of oxygen *2p* orbitals. The conduction band begins at around 0.4 eV but the density of states is very low up to a peak feature at about 2.7 eV. There is also a second peak feature at 4.0 eV. This band is comprised mostly of tungsten *5d* orbitals, as in the tungsten oxides and bronzes, but in these hybrid compounds there is an additional oxygen *2p* component to this band. The apical oxygen atom contributes to the first peak feature and the planar oxygen atoms contribute to the second. Above 4.5 eV lie the organic anti-bonding orbitals. The band structure in the vicinity of the Fermi level (i.e. valence and conduction bands) is virtually identical for the three different organic intercalates. As expected the organic molecule does not participate in electronic conduction and the compound is an insulator. Features in the calculated band structure relate very closely to the band gap as determined by UV-visible spectroscopy [50]. Powder spectra of the hybrids indicate a shift in the absorption edge from 2.6-2.8 eV for WO_3 to 4.1 eV for the hybrids [18]. There was no systematic variation amongst the positions of the absorption edges for the hybrid materials. It appears likely that the features in the UV-visible powder spectra correspond to indirect band gaps, which are displayed in the calculated density of states spectra as peak features in the valence band, where the occupancy of the band suddenly increases.

SUMMARY

A number of tungsten oxide-based systems have been studied using *ab initio* computation techniques. Hexagonal and cubic alkali tungsten bronzes exhibit trends in cell sizes which agree well with experimental data. The band structure and charge density plots of these show that the intercalated alkali atom (with the exception of hydrogen) donates its electron to the conduction band. An in-depth study of the partially doped cubic sodium bronze system showed the progressive movement of the Fermi level into the conduction band. However it is suspected that in the experimental system the onset of metallic conductivity is associated with or induced by a phase change not accounted for in these calculations. A transition to a conducting state is also observed experimentally in oxygen-deficient tungsten trioxide. This is modelled well by the calculations, as are the changing cell dimensions. The free energy indicates that a slight deficit of oxygen renders tungsten trioxide more stable than the exactly stoichiometric form, which is also observed experimentally. Lastly three tungsten-oxide/organic hybrids with simple α,ω-diaminoalkane molecules were studied. They are energetically stable and exhibit many similarities in the band structure to that of the parent cubic tungsten trioxide. The amines are protonated to form ammonium groups and the undoped diammoniumalkane hybrids are calculated to be electrically insulating.

ACKNOWLEDGMENTS

The authors would like to acknowledge the financial assistance from the New Zealand Foundation of Research Science and Technology (Contract number: IRLX0201), The Royal Society of New Zealand Marsden Fund, and the MacDiarmid Institute for Advanced Materials and Nanotechnology (Victoria University, New Zealand).

[1] M. Figlarz, Prog. Solid State Chem. **19**, 1 (1989).
[2] B. Mourey, M. Hareng, B. Dumont, J. Desseine, and M. Figlarz, Eurodisplay Proc. p. 223 (1984).
[3] J. Bailar, H. Emeleus, R. Nyholm, and A. Trotman-Dickenson, eds., *Comprehensive Inorganic Chemistry* (Pergamon, Oxford, 1973), vol. 4, chap. 50: Tungsten Bronzes, Vanadium Bronzes and Related Compounds.
[4] J. Guo, K. Reis, and M. Whittingham, Solid State Ionics **53**, 315 (1992).
[5] A. Coucou and M. Figlarz, Solid State Ionics **28-30**, 1762 (1988).
[6] J. Bailar, H. Emeleus, R. Nyholm, and A. Trotman-Dickenson, eds., *Comprehensive Inorganic Chemistry* (Pergamon, Oxford, 1973), vol. 3, chap. 36: Chromium, Molybdenum and Tungsten, p. 623.
[7] S. Haydon and D. Jefferson, J. Solid State Chem. **168**, 306 (2002).
[8] C. Grenthe and M. Sundberg, J. Solid State Chem. **167**, 402 (2002).
[9] M. Straumanis, J. Am. Chem. Soc. **71**, 679 (1949).
[10] W. Gardner and G. Danielson, Phys. Rev. **93**, 46 (1954).
[11] R. Goldner, T. Haas, G. Seward, K. Wong, P. Norton, G. Foley, G. Berera, G. Wei, S. Schulz, and R. Chapman, Solid State Ionics **28-30**, 1715 (1998).
[12] K. Bange, Sol. En. Mat. Sol. Cells **58**, 1 (1999).
[13] C. Lampert, Sol. En. Mat. Sol. Cells **52**, 207 (1998).
[14] H. Shanks, Solid State Comm. **15**, 753 (1974).
[15] S. Lee, H. Cheon, C. Tracy, A. Mascarenhas, A. Czanderna, and S. Deb, Appl. Phys. Lett. **75**, 1541 (1999).
[16] A. Georg, W. Graf, and V. Wittwer, Sol. En. Mat. Sol. Cells **51**, 353 (1998).
[17] O. Glemser and H. Sauer, Z. anorg. Chem. **252**, 144 (1943).
[18] S. Chong, B. Ingham, and J. Tallon, Curr. Appl. Phys. **4**, 197 (2004).
[19] B. Ingham, S. Chong, and J. Tallon, Mat. Res. Soc. Symp. Proc. **775**, 165 (2003).
[20] A. Walkingshaw, N. Spaldin, and E. Artacho, Phys. Rev. B. **70**, 165110 (2004).
[21] J. Perdew, K. Burke, and M. Ernzerhof, Phys. Rev. Lett. **77**, 3865 (1996).
[22] G. Kresse and J. Hafner, Phys. Rev. B **47**, RC558 (1993).
[23] G. Kresse, Ph.D. thesis (Technische Univerität Wien) (1993).
[24] G. Kresse and J. Furthmüller, Comput. Mater. Sci. **6**, 15 (1996).
[25] G. Kresse and J. Furthmüller, Phys. Rev. B **53**, 11169 (1996).
[26] D. Vanderbilt, Phys. Rev. B **41**, 7892 (1990).
[27] G. Kresse and J. Hafner, J. Phys.: Condens. Matter **6**, 8245 (1994).
[28] D. Bullett, J. Phys. C **16**, 2197 (1983).
[29] B. Brown and E. Banks, J. Am. Chem. Soc. **76**, 963 (1954).
[30] R. Roth and J. Waring, J. Res. Natl. Bur. Stand. **A 70**, 281 (1966).
[31] O. Glemser and C. Naumann, Z. anorg. Chem. **265**, 288 (1951).
[32] B. Chamberland, Inorg. Chem. **8**, 1183 (1969).
[33] V. Goldschmidt, Naturwiss. **14**, 477 (1926).
[34] G. Aylward and T. Findlay, *SI Chemical Data* (Jacaranda Wiley Ltd., Brisbane, 1994).
[35] B. Hobbs and A. Tseung, J. Electrochem. Soc. **119**, 580 (1972).
[36] F. D. Quarto, A. D. Paola, and C. Sunseri, Electrochim. Acta **26**, 1177 (1981).
[37] K. Gesheva, A. Szekeres, and T. Ivanova, Sol. En. Mat. Sol. Cells **76**, 563 (2003).
[38] L. Ottaviano, F. Bussolotti, L. Lozzi, M. Passacantando, S. L. Rosa, and S. Santucci, Thin Solid Films **436**, 9 (2003).
[39] O. Khyzhun, Y. Solonin, and V. Dobrovolsky, J. Alloys Compounds **320**, 1 (2001).
[40] A. Hjelm, C. Granqvist, and J. Wills, Phys. Rev. B **54**, 2436 (1996).
[41] F. Cora, M. Stachiotti, and C. Catlow, J. Phys. Chem. B **101**, 3945 (1997).
[42] B. Brown and E. Banks, Phys. Rev. **84**, 609 (1951).
[43] E. Brimm, J. Brantley, J. Lorenz, and M. Jellinek, J. Am. Chem. Soc. **73**, 5427 (1951).
[44] G. Rieck, *Tungsten and its Compounds* (Pergamon, Oxford, 1967).
[45] A. Magneli, Ark. Kemi **1**, 513 (1950).
[46] A. Magneli, Ark. Kemi **1**, 223 (1949).
[47] J. Booth, T. Ekstrom, E. Iguchi, and R. Tilley, J. Solid State Chem. **41**, 293 (1982).
[48] J. Szymanski and A. Roberts, Can. Mineral. **22**, 681 (1984).
[49] D. Mitzi, Prog. Inorg. Chem. **48**, 1 (1999).
[50] B. Ingham, S. Chong, and J. Tallon, Curr. Appl. Phys. **4**, 202 (2004).